Appl. Phys. B 61, 429–437 (1995)

Applied Physics B Lasers and Optics

Continuous-wave mode-locked solid-state lasers with enhanced spatial hole burning

Part I: Experiments

B. Braun, K.J. Weingarten, F.X. Kärtner, U. Keller

Swiss Federal Institute of Technology, Institute of Quantum Electronics, ETH Hönggerberg HPT, CH-8093 Zürich, Switzerland (Fax: + 41-1/633-1059, E-mail: KAERTNER@iqe.ethz.ch)

Received: 12 April 1995/Accepted: 7 June 1995

Abstract. We systematically investigate the difference between both actively and passively mode-locked lasers with Gain-at-the-End (GE) and Gain-in-the-Middle (GM) at the example of Nd:YLF lasers. The GE laser generates pulse widths approximately three times shorter than a comparable GM cavity. This is due to enhanced Spatial Hole Burning (SHB) which effectively flattens the saturated gain and allows for a larger lasing bandwidth compared to a GM cavity. We first investigate enhanced SHB by measuring the cw mode spectrum, where we have observed that the mode spacing in GE cavities depends primarily on the crystal length. This was also confirmed for a Nd:LSB crystal, where the pump absorption length was significantly shorter than the crystal length. In mode-locked operation, pulse widths of 4 ps for passive mode locking and 5 ps for active mode locking are demonstrated with GE cavities, compared to 11 ps for passive and 17 ps for active mode locking with GM cavities. Additionally, the time–bandwidth product for the GE cavity is approximately twice the ideal product for a sech^2 pulse shape and cannot be improved by dispersion compensation alone, while the GM cavity has nearly ideal time–bandwidth-limited performance. The results for the GM cavity compare well to existing theories taking into account the added effect of pump-power-dependent gain bandwidth which increases the bandwidth of Nd:YLF from 360 to > 500 GHz. In a following paper [1] (called Part II) a rigorous theoretical treatment of the effects due to SHB will be presented.

PACS: 42.60; 42.55; 42.65

Picosecond pulse generation using lamp-pumped actively mode-locked solid-state lasers with homogeneously broadened gain is well described by the Kuizenga-Siegman theory [2, 3]. For several years now, however, end-pumped (often diode-pumped) mode-locked lasers have demonstrated pulse widths significantly shorter than those predicted by the Kuizenga-Siegman mode-locking theory. For example, actively mode-locked lamp-pumped lasers generate typical pulse widths of 80–100 ps in Nd:YAG and 30–50 ps in Nd:YLF. In contrast, a significant decrease in pulse width was observed with the introduction of diode-pumped actively mode-locked lasers [4–6], which produced pulses as short as 7 ps in Nd:YLF [5], and in the case of a diode-pumped Nd:BEL laser pulses as short as 2.9 ps [7]. These results cannot be well-explained by the Kuizenga-Siegman mode-locking theory, which neglects such effects as SHB and Self-Phase-Modulation (SPM). In general, longitudinally pumped solid-state lasers experience stronger SPM compared to flashlamp-pumped lasers due to their smaller cavity mode in the gain medium, and SPM could significantly broaden the pulse spectrum resulting in shorter pulses [8]. However, based on our experimental and theoretical investigations, we believe that SHB is the key effect responsible for pulse shortening in end-pumped lasers.

The general phenomenon of SHB in lasers is well-established [9, 10]. The effects of SHB for end-pumped mode-locked lasers were suggested by several authors in the last few years [11, 12]. More recently, we presented evidence that short-pulse generation is specifically due to SHB in GE lasers [13, 14]. Flood et al. published experiments and analyses showing that the mode-locked pulse width depends on the position of the gain region in the cavity [15].

In this paper (Part I), we show by a systematic experimental study that the effects due to SHB significantly reduce the pulsewidth in both actively and passively mode-locked solid-state lasers. The effects of SHB are most pronounced when the gain region is at one end of the laser cavity and when its length is on the order of the pulse width. However, SHB not only shortens the pulsewidth, but also increases the time–bandwidth product with respect to a sech^2 or Gaussian pulse shape. We typically obtained pulses with twice the ideal time–bandwidth product of a sech^2 pulse shape, and this value could not be improved by dispersion compensation inside the cavity. This is due to the flat saturated gain which results in a non-trivial, i.e. non-gaussian or sech^2 shape of the

mode-locked lasing spectrum. Furthermore, we measured that the mode-locking build-up time with enhanced SHB is strongly reduced for both active and passive mode-locking, if a sufficiently large mode-locking driving force is provided. In Part II of this paper [1], we develop a laser model including the effects due to SHB that explains most of the experimental results presented here.

1 Simple description of "enhanced" spatial hole-burning

Here, we give a simplified schematic picture as to why a laser cavity with GE experiences "enhanced" SHB compared to laser cavities with GM. A laser with an ideal homogeneously broadened gain medium in a unidirectional ring laser will only lase in one axial mode [16] and experiences no SHB. For a standing-wave cavity, the first mode to lase sets up a standing wave in the laser gain (Fig. 1a). A second axial mode will then see a space-dependent gain with lower gain at the peaks of the standing wave due to gain saturation, and higher gain at nodes of the standing wave where the gain is unsaturated (Fig. 2).

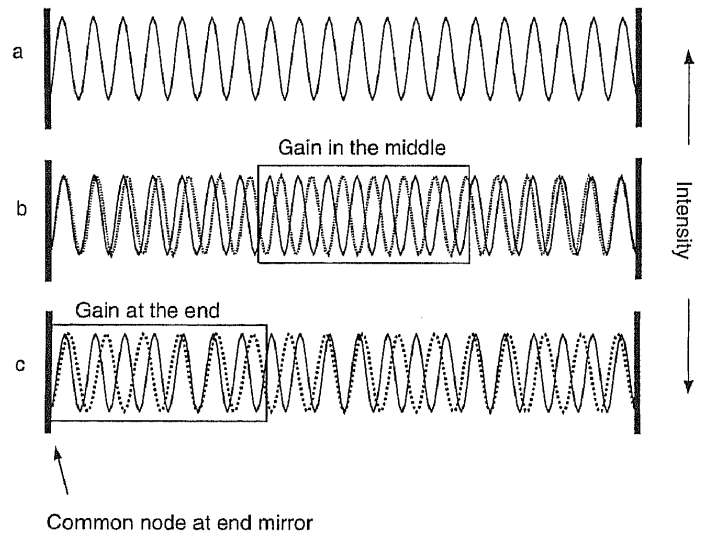

Fig. 1a–c. Schematic description of enhanced SHB: (**a**) Standing-wave pattern of one axial mode inside a linear laser cavity; (**b**) an adjacent axial mode fills-in the undepleted gain regions of a GM cavity; (**c**) The axial mode that can fill-in the undepleted gain regions of a GE cavity has a much larger frequency difference to the first mode

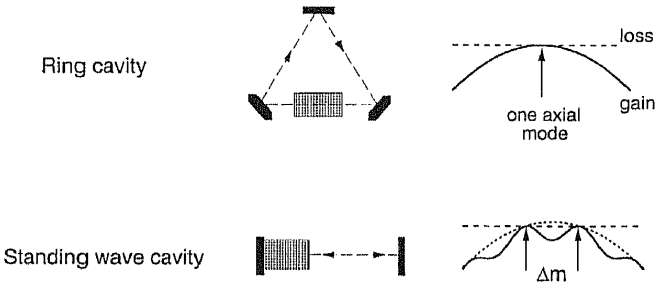

Fig. 2. In a ring cavity, the laser is ideally homogeneously broadened and the first mode to lase saturates the entire gain region. In a standing-wave cavity, SHB causes an effective periodic modulation of the gain. As the gain medium is moved closer to end of the cavity, the spacing between lasing modes Δm increases

The boundary condition at the end of the standing-wave cavity requires a common node for all axial modes. Then, with a gain medium in the middle of the laser cavity and one mode running, the intensity modulation of the adjacent axial mode will be exactly 180° out of phase with the first mode in the middle of the cavity and experiences the largest spatial overlap with the remaining undepleted gain (Fig. 1b). With GM then, adjacent axial modes typically will lase and deplete the available gain.

However, the frequency separation between modes that fill the available spatial holes increases as the gain region is moved from the middle of the cavity to the end of the cavity. This is the well-known effect that the position of the gain affects the standing-wave pattern [17]. It has been used to increase the performance of single-frequency micro-chip lasers [18, 19]. With the gain medium at the end mirror, the next axial mode to lase has a much larger frequency difference (Fig. 1c) compared to GM. In addition, the closer the gain medium is placed to the cavity end, the more modes are required to fully deplete the gain due to the common boundary condition, i.e., the common node at the end of the cavity. For this case, we experimentally (and theoretically in Part II [1]) demonstrate that pumping the laser far above threshold results in a much broader overall cw-lasing bandwidth with a large frequency separation between the lasing modes, which ultimately allows for shorter pulse generation.

2 Experimental setup

The outlines of the two types of cavities (GE and GM) are shown in Fig. 3. Both lasers used π-oriented Nd:YLF lasing at 1047 nm. For the GE cavity (Fig. 3a), the Nd:YLF crystal is cut at Brewster's angle on one side and is a flat on the other, with the standard (Anti-Reflection) AR-coating for the pump wavelength and (High Reflector) HR-coating for the lasing wavelength. The center length of the crystal L_c is 4.5 mm. In the GM cavity (Fig. 3b), a Nd:YLF crystal plate with a thickness of L_c of 5 mm is inserted at Brewster's angle. The Nd doping is 1.5% in both cases. The pump source for the Nd:YLF laser was a cw Ti:Sapphire laser at a wavelength of 793 nm, resulting in an absorption depth l_a of 2.3 mm. The measured spot radius of the pump beam in the tangential plane is 20 μm for both cavities.

The additional design parameters of the GE Nd:YLF cavity (Fig. 3a) are: $L_1 = 11.1$ cm, $L_2 = 48.2$ cm, $R_1 = 20$ cm, resulting in a longitudinal mode spacing or pulse repetition rate of 250 MHz. The angle θ_1 is 13.5° to compensate the astigmatism of the Brewster-cut laser crystal. The mode radius in the laser crystal has been calculated to be $70 \times 100\ \mu m^2$ in the sagital and tangential plane, respectively, using the *ABCD* matrix formalism. At the output coupler the mode radius was calculated to be $360 \times 360\ \mu m^2$. For passive modelocking, the flat end-mirror was replaced with a curved mirror of radius $R_2 = 10$ cm and an antiresonant Fabry-Perot Saturable Absorber (A-FPSA) [20, 21]. With a length $L_3 = 5.5$ cm, we obtained a calculated beam radius of $30 \times 30\ \mu m^2$ on the A-FPSA. L_3 is adjusted for operation in the middle of the stability regime which was confirmed experimentally

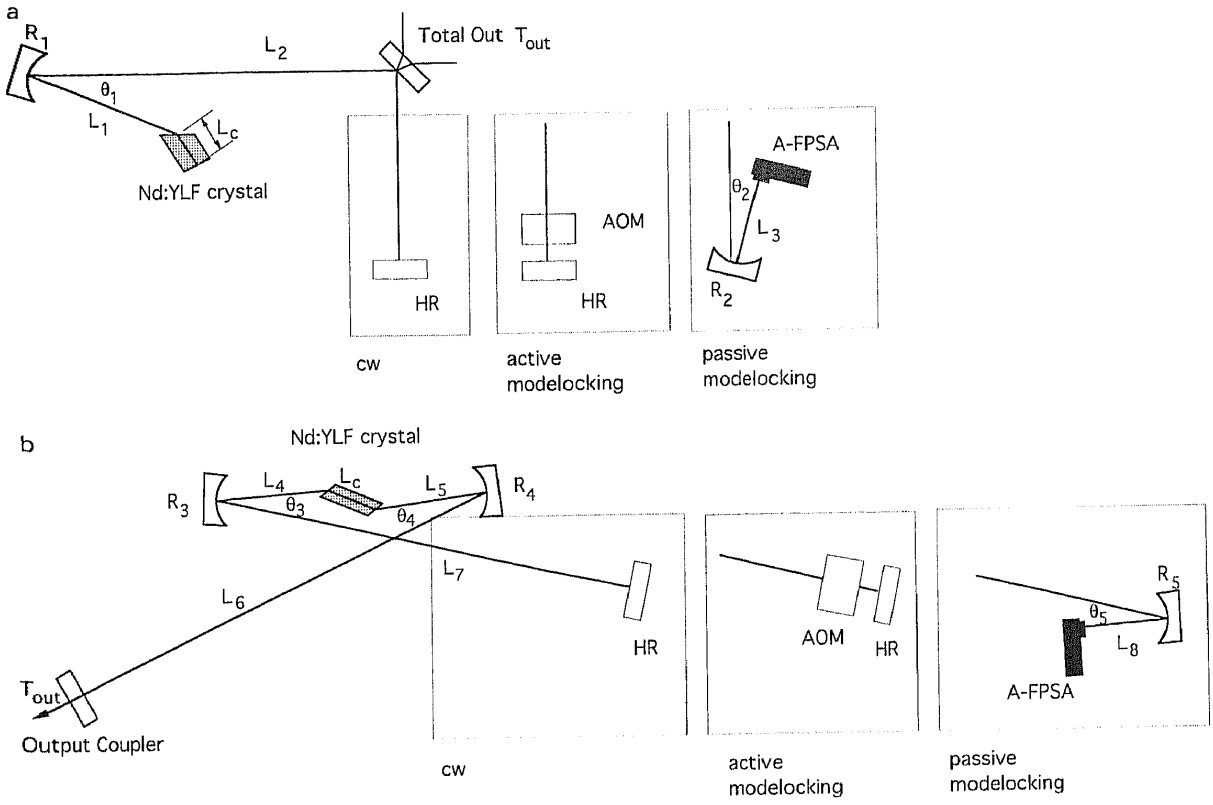

Fig. 3a, b. Laser cavity design and parameters for two standing-wave cavities: (**a**) GE cavity and (**b**) GM cavity. AOM is an acousto-optic mode-locker. The laser mode radius in the crystal is 130 μm by 90 μm (calculated) for the GM cavity and 100 μm by 70 μm (calculated) for the GE cavity. In both cases, the pump radius in the tangential plane was approximately 20 μm at 793 nm from a Ti:Sapphire laser. Both laser cavities have a round-trip length of 1.2 m corresponding to a repetition rate of 250 MHz and a 2.5% total output coupler

by moving the A-FPSA sample in both directions until it stopped lasing, and then centering its position between these two stability limits.

The design parameters for the GM cavity (Fig. 3b) are: $L_4 = L_5 = 9.7$ cm, $L_6 = L_7 = 20$ cm, $\theta_3 = \theta_4 = 9.6^\circ$ and $R_3 = R_4 = 15$ cm. The calculated beam radius inside the laser crystal and at the output coupler are $90 \times 130\ \mu m^2$ and $200 \times 200\ \mu m^2$ in the sagital and tangential plane, respectively. For passive mode locking, we again replaced one flat end mirror with a curved mirror of radius $R_5 = 10$ cm, which focuses the resonator mode down to a calculated spot radius of $30 \times 30\ \mu m^2$ on the A-FPSA. The other numbers for distances and angles are changed to $L_4 = 3.3$ cm, $L_5 = 8.8$ cm, $L_6 = 17.8$ cm, $L_7 = 23.4$ cm, $L_8 = 6.1$ cm, $\theta_3 = \theta_4 = 10^\circ$ and $\theta_5 = 7.2^\circ$. In this case we also operate the laser in the middle of the cavity stability regime.

3 CW lasing properties of both cavities

For the cw cavities, we measured the slope efficiency, the relaxation oscillation frequency and the laser spectrum. The slope efficiency of the GE cavity is 55% with a lasing threshold of ≈10 mW and an output coupler transmission of 2.5%. The GM cavity has a slope efficiency of 52% with the same output coupling of 2.5% and a slightly higher threshold pump power of ≈15 mW due to the larger pump mode area (i.e. the Brewster-angled orientation of the Nd:YLF crystal increases the pump radius in the tangential plane for the GM cavity). Thus, both cavities have similar cw lasing characteristics.

The relaxation oscillation frequency was measured to determine the laser's small-signal gain [22]. In Fig. 4a, the measured relaxation oscillation frequencies for the different cavities are shown as a function of absorbed pump power. From these data, we can calculate the small-signal gain [22] (Fig. 4b), using a measured upper state lifetime of 450 μs, the measured longitudinal mode spacing of 250 MHz, and an estimated cavity loss of ≈0.5% for the cw running cavities, additional 0.5% for A-FPSA mode locking, and 1% for acousto-optic mode locking. The small-signal gain will become important for the comparison of the mode-locking build-up time with and without enhanced SHB.

The laser spectrum is measured using a scanning Fabry-Perot interferometer. Figure 5 shows a typical spectrum of the GE and the GM cavity. The laser in the GM-cavity configuration always shows a narrow spectrum, which cannot be resolved by the scanning Fabry-Perot. In contrast, the Nd:YLF laser with the GE cavity has a broad cw spectrum consisting typically of 6–8 longitudinal modes, each spaced by approximately 23 GHz. The number of lasing longitudinal modes increases with increasing pump power (Fig. 6).

To measure the spacing Δm between the lasing modes as a function of the length of the gain medium for the GE cavity, the length l_g of the gain medium was varied from 4.0 to 5.2 mm for the Nd:YLF by moving the crystal perpendicular to the laser between the short and the long

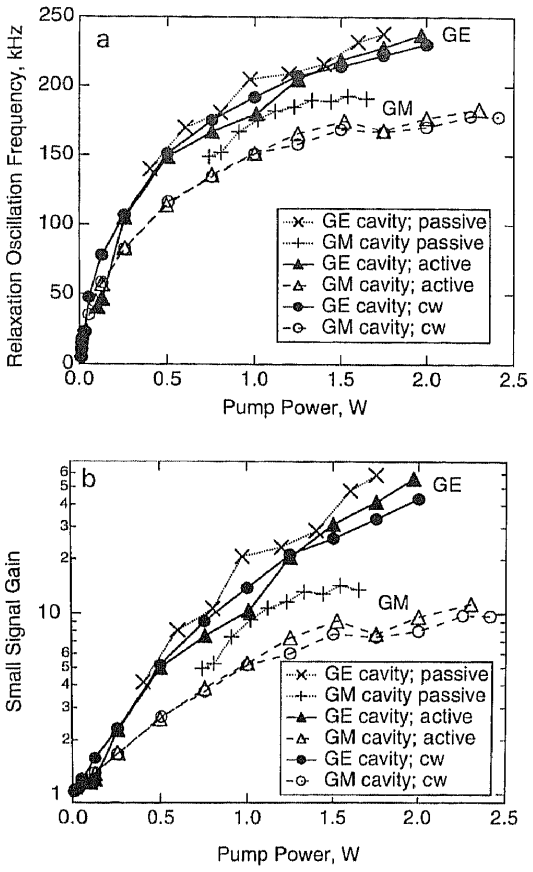

Fig. 4. **a** Measured relaxation oscillation frequencies for the different cavities. **b** Small-signal gain calculated from the relaxation oscillation [22]

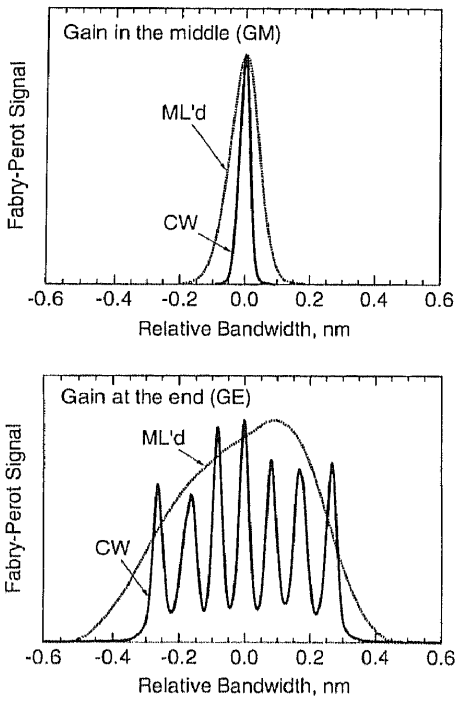

Fig. 5. Comparison of the cw and mode-locked spectra for both cavities at an intracavity intensity of approximately 60 kW/cm^2 inside the Nd:YLF crystal. The resolution of the Fabry-Perot spectrum analyser limits the width of the measured cw spectrum of the GM cavity and also the width of the individual axial modes seen in the cw spectrum of the GE cavity

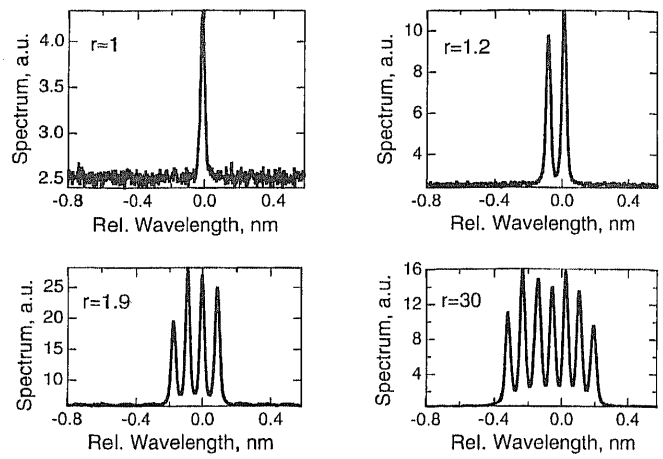

Fig. 6. CW spectra for different pump parameters r (times above threshold)

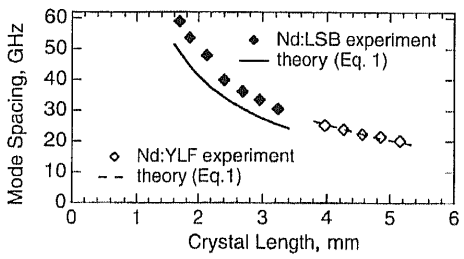

Fig. 7. Measured and calculated mode spacing to (1) as a function of the crystal length for different absorption constants. The measurements are done both with a Nd:YLF ($\lambda = 1047$ nm, $n = 1.47$ [39], $1/\alpha = 2.3$ mm) as well as with a Nd:LSB crystal ($\lambda = 1062$ nm, $n = 1.82$[23], $1/\alpha = 280$ μm)

edge of the crystal. We also measured the mode spacing using a 10% doped Nd:LSB crystal [23, 24] which has an absorption length of $l_a = 1/\alpha = 280$ μm, significantly shorter than the crystal length, which was varied from 1.7 to 3.2 mm. The experimental results for pumping far above threshold are shown in Fig. 7. We can see that the doubled gain length results in a reduction of the spacing of the lasing modes by a factor of 2, even for the Nd:LSB laser which has an absorption depth roughly ten times shorter than the laser crystal. Thus, we find experimentally that the periodic spacing of the lasing longitudinal modes is approximately given by the effective free spectral range $\Delta f_{\mathrm{FSR,g}}$ of the gain medium

$$\Delta f_{\mathrm{FSR,g}} = \frac{c}{2nl_g} \tag{1}$$

where n is the refractive index of the gain medium with length l_g. The formula is in good agreement with the experiment, even for Nd:LSB up to 15%, as can be seen from Fig. 7. This result is slightly surprising, since one would expect that effects due to SHB would more strongly depend on the length of the pumped gain region, which depends on the absorption depth. However, because the available gain is determined by an overlap integral of the mode with the spatial gain profile over the entire crystal, it can be shown that (1) is quite accurate as long as the absorption depth l_a is more than approximately one-tenth

of the length of the gain material l_g. A detailed discussion of this effect together with numerical simulations is given in Part II of this paper [1].

4 Actively and passively mode-locked lasers without SHB

We investigated active and passive mode locking with the GM cavity, where the pulses experience no SHB. Both the Kuizenga-Siegman [2,3,25] and the Haus theory [8], which includes SPM, cannot fully explain the experimental results for active mode locking. Other effects such as Kerr-Lens Mode locking (KLM) and thermal lensing are negligible. We demonstrate, however, that the gain bandwidth is increasing with increased pump power due to heating effects. Taking into account this phonon-broadened gain bandwidth, a better agreement with the experimental result is obtained. In the case of passive mode locking, we obtained good agreement with the "fast saturable absorber model" from Haus [26].

4.1 *Active mode locking*

We actively mode-locked the GM laser with an acousto-optic modulator, and routinely achieved pulses as short as 16 ps (Fig. 8). The Kuizenga-Siegman theory [2,3,25] predicts a FWHM pulse duration given by

$$\tau_p = 0.446 \sqrt[4]{\frac{g}{M}} \sqrt{\frac{1}{f_m \Delta f_g}}, \tag{2}$$

resulting in $\tau_p \approx 29$ ps, where the saturated power gain of the laser is in the steady state given by $2g \approx T_{out} + l \approx (0.025 + 0.015)$; $M = 0.14$ is the measured modulation depth of the acousto-optic modulator defined by the

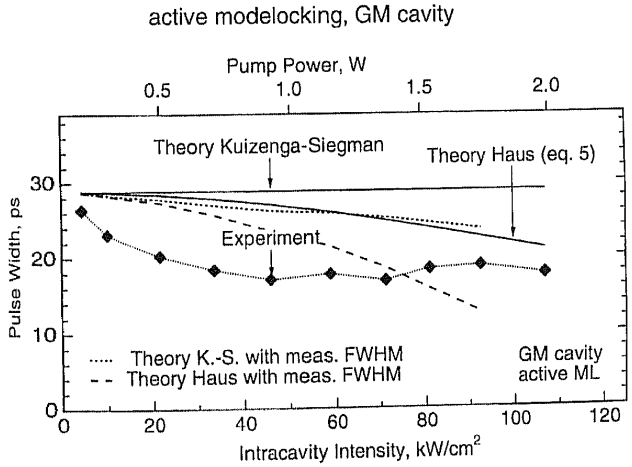

Fig. 8. Actively mode-locked GM Nd:YLF laser ($\lambda = 1047$ nm). Comparison of the measured pulsewidth with the calculated one using the Kuizenga-Siegman (2) and Haus' theory (11) with $\Delta f_g = 360$ GHz [27] (*solid line*) and the measured intensity-dependent lasing gain bandwidth (Fig. 9) (*dashed line*). The intracavity intensity is calculated with respect to the mode size in the crystal (i.e., $90 \times 130\ \mu m^2$). The other experimental parameters are $g = 0.020$, $M = 0.14$, $f_m = 250$ MHz, $n_2 = 1.43 \times 10^{-16}$ cm²/W [40], and $l_g = 5$ mm

amplitude loss coefficient of the mode-locker $q(t) = M[1 - \cos(2\pi f_m t)]$; $f_m = 250$ MHz is the modulation frequency, which is also the free spectral range of the cavity; $\Delta f_g = 360$ GHz [27] is the FWHM gain bandwidth of Nd:YLF; and l is the amplitude loss coefficient per round trip. Figure 8 shows that the intensity-independent pulsewidth predicted by Kuizenga-Siegman (2) cannot explain our experimental results, even though an excellent agreement at low intensity is obtained.

Following the theory of Haus and Silberberg [28], we can extend the Kuizenga-Siegman mode-locking theory by including SPM, but still assuming a homogeneously broadened and Lorentzian line profile for the laser transitions. The master equation for the mode-locked laser is given by

$$T_R \frac{\partial}{\partial T} A(T,t) = i\delta |A(T,t)|^2 A(T,t) + \left[g\left(1 + \frac{1}{\Omega_g^2} \frac{\partial^2}{\partial t^2}\right) - l_c - q(t) \right] A(T,t), \tag{3}$$

where $A(T,t)$ is the slowly varying envelope of the pulse, $|A(T,t)|^2$ the intracavity intensity, T_R the cavity roundtrip time, δ the self-phase modulation coefficient given by $\delta = 2n_2 l_g 2\pi/\lambda$, with n_2 the nonlinear refractive index, l_g the length of the gain material, and λ the vacuum lasing wavelength, g is the saturated amplitude gain coefficient per round trip, l_c the amplitude loss coefficient per round trip, $\Omega_g = 2\pi\Delta f_g/2$ is the HWHM gain bandwidth in radians, with Δf_g the FWHM gain bandwidth in Hertz. The acousto-optic mode-locker gives a loss modulation amplitude coefficient

$$q(t) = M[1 - \cos(\omega_m t)], \tag{4}$$

where M is the modulation depth and ω_m the modulation frequency ($\omega_m = 2\pi f_m$) [2,28]. Equation (3) does not include the effects of Group-Velocity Dispersion (GVD) because our pulse durations are in the picosecond regime. The changes in the pulse per round trip (coarse time scale T) are assumed to be small, and the modulator frequency is assumed to perfectly match the round-trip frequency. An ansatz for the stationary solution is made with a chirped Gaussian:

$$A(T,t) = \sqrt{I_p} \exp\left[-\frac{1}{2} \frac{t^2}{\tau^2} (1 - ix) \right], \tag{5}$$

where $I_p = |A(T,0)|^2$ is the peak intensity of the pulse. By using the ansatz given in (5) with (3) and (4), we obtain the following FWHM pulse duration:

$$\tau_p = 1.66\,\tau = 1.66 \sqrt[4]{\frac{D_g}{\frac{M\omega_m^2}{2} + \frac{\Phi_0^2}{4D_g}}}, \tag{6}$$

where D_g is the gain dispersion

$$D_g = \frac{g}{\left(2\pi \frac{\Delta f_g}{2}\right)^2}, \tag{7}$$

and Φ_0 is the nonlinear phase shift within one round trip

$$\Phi_0 = 2\frac{2\pi}{\lambda} n_2 I_p l_g. \tag{8}$$

Because the confocal parameter of the cavity mode is longer than the crystal length, we assume the peak intensity to be constant throughout the gain crystal. The chirp of the pulse increases with increasing SPM.

At this point, however, we have not discussed the stability of the solution given in (6) because it would predict arbitrary pulse shortening with increasing SPM. It is important to remember that the master equation is a linearized description of the mode-locking problem and is only valid for $\Phi_0 \ll 2\pi$. This linearization is justified, however, because numerical simulations have shown that the laser becomes unstable with increasing SPM, and generally only a pulse shortening by a factor of ≈ 2 can be achieved before the laser runs unstable [8]. In contrast, in the negative GVD regime the pulse shortening can be much larger [29].

A comparison between the theoretical prediction (6) and the experimental results shows that the pulse duration is predicted reasonably well, but that the pulse duration initially decreases faster than expected for increasing intensity (Fig. 8). There are several possible explanations for this effect. One possibility is thermal lensing, which is very small for Nd:YLF [30]. Additionally, the cavity mode area would increase with increasing intensity in this cavity design if it were significant. This would cause an increase in pump threshold, thus, lower small-signal gain and longer pulses, which contradicts our experimental observation (Fig. 8).

Another possible effect is KLM. To estimate the effect of KLM, the mode-size reduction due to self-focusing in the gain material is determined with $ABCD$ matrix calculations [31]. From the change in mode area ΔA, the variation in gain Δq due to "soft aperturing" can be calculated with (6) of [21]. Given the parameters of our cavity, the maximum change of the gain due to KLM for a peak intensity of 10 kW is on the order of 1×10^{-5}. We therefore conclude that the effects of KLM are negligible here.

So far, we have assumed that the gain bandwidth is constant. However, we have observed that the measured fluorescence spectrum increases as a function of pump power (Fig. 9a). We observe both a red shift of the center wavelength by approximately 34 GHz/W of pump power and a fluorescence linewidth broadening from 360 to as high as 550 GHz. Our measured low-intensity linewidth corresponds to the value listed by Kaminskii [27]. The pump is focused to a radius of 20 μm within the Nd:YLF crystal of 5 mm length and confocal focusing length of 4.7 mm. A simple calculation with (2) of [32] shows that the temperature within the 20 μm pump-area radius is approximately constant. Therefore, we can assume that the observed linewidth broadening (Fig. 9a) is a homogeneous phonon broadening, and the previously discussed mode-locking models should still apply. However, it is important to note that in the case of diode-laser pumping, the pump area more closely matches the mode area, which would introduce significant inhomogeneous broadening

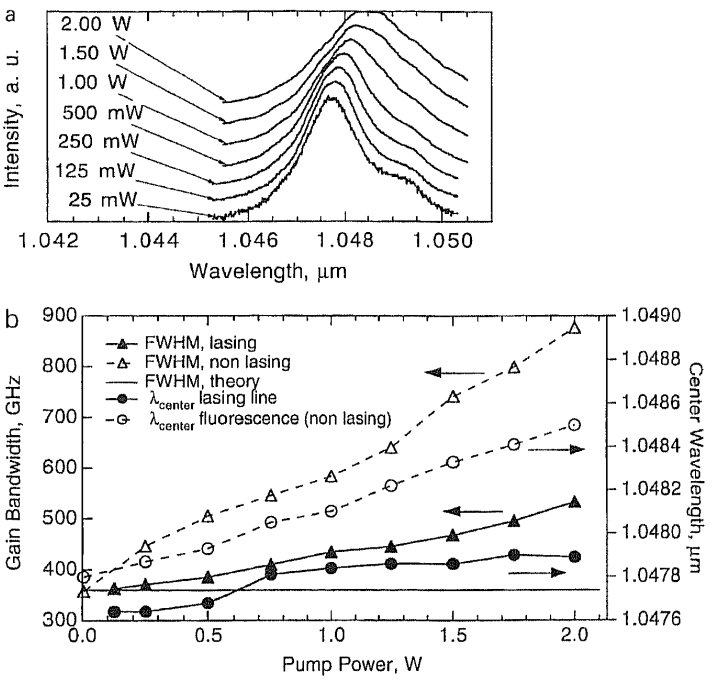

Fig. 9. a Pump-intensity-dependent fluorescence bandwidth of the Nd:YLF laser. **b** Fluorescence bandwidth fitted to a Lorentzian lineshape and center wavelength shift for the Nd:YLF crystal under lasing (3.0% output coupler, GM cavity) and non-lasing conditions

due to the temperature dependence in the gain area. To take into account the intensity-dependent linewidth, we measured the linewidth while the laser was lasing with a 3.0% output coupler (Fig. 9b). As expected, under lasing conditions we observe less broadening for a given pump power because stimulated emission reduces the upper laser state lifetime by the factor r, compared to the spontaneous lifetime, where r is the amount the laser is above threshold. This produces less heating for a given pump power because the probability for higher-order phonon-assisted recombination processes is strongly reduced. The intensity-dependent fluorescent lasing gain bandwidth was then taken into account for our mode-locking models (2, 6) (Fig. 8). The agreement is better and fits within the calculated experimental error of about ± 20%. It is also possible that residual inhomogeneous broadening could be responsible for the initial faster pulse shortening (Fig. 8). At high intensities Haus' theory (6) predicts even shorter pulses, but these pulsewidths are not stable, as discussed above.

4.2 Passive mode locking

For passive mode locking of the GM cavity (Fig. 3b), we used an A-FPSA [20, 21], which consists of an InGaAs/GaAs saturable absorber MBE grown at low-temperature of 260°C, having a carrier lifetime τ_c of 3.8 ps and an AR-coated saturation fluence $E_{sat}^0 = 79\ \mu J/cm^2$ [33]. An evaporated dielectric top reflector R_t of 95.5 ± 0.5% is used which gives an effective saturation fluence of $E_{sat}^{eff} = (4.6 \pm 0.5)$ mJ/cm^2 ([33], Eq. (14)) and therefore, an effective saturation intensity of $I_{sat}^{eff} = E_{sat}^{eff}/\tau_c = (1.2 \pm 0.13)$GW/cm^2. This determines a maximal

nonlinear reflectivity change ΔR of $0.55 \pm 0.05\%$ ([33], Eq. (19) with $R_0 R_{ns} = 0.4$ from Fig. 5a, $\Delta R_{ns} = 0.325$ from Fig. 7b, and $R_{ns} = 1 - \Delta R_{ns} = 0.675$). For small reflectivity changes we can assume that $1 - \Delta R = \exp(-2q_0) \approx 1 - 2q_0$, i.e., $\Delta R \approx 2q_0$. The maximal nonlinear amplitude loss coefficient is $q_0 = (2.75 \pm 0.25) \times 10^{-3}$, which will be used again in Part II of this paper [1].

The pulse shortening with increasing intracavity power (Fig. 10) is obtained due to increased absorption bleaching in the A-FPSA, which increases the nonlinear reflectivity [33]. The short carrier lifetime with respect to the typical pulse lengths for the GM cavity ($\tau_p \geq 11$ ps) allows us to apply Haus' theory for fast saturable absorber mode locking [26] with the master equation (3) without SPM (i.e., $\delta = 0$). The saturable absorber produces a self-amplitude loss coefficient given by [26]

$$q(t) = q_0 - \gamma |A(t)|^2 = q_0 - \gamma I(t), \tag{9}$$

where $I(t)$ is the incident intensity on the saturable absorber and γ the self-amplitude-modulation coefficient. In the limit of a fast saturable absorber, we can assume that

$$q(t) = \frac{q_0}{1 + I(t)/I_{sat}^{eff}} \approx q_0[1 - I(t)/I_{sat}^{eff}], \quad \text{for } I(t) \ll I_{sat}^{eff}. \tag{10}$$

Therefore, $\gamma = q_0/I_{sat}^{eff}$. The solution of the fast saturable absorber mode-locking model [26] then predicts a sech^2 pulse shape with a FWHM pulsewidth of

$$\tau_p = 1.763 \frac{4D_g}{\gamma W}, \tag{11}$$

where D_g is the gain dispersion (7) and W the pulse energy density incident on the A-FPSA. The result for a constant gain bandwidth of 360 GHz [27] and the intensity-dependent lasing gain bandwidth (Fig. 9b) is plotted in Fig. 10 together with the experimental data, which gives the correct order of magnitude and the general behavior.

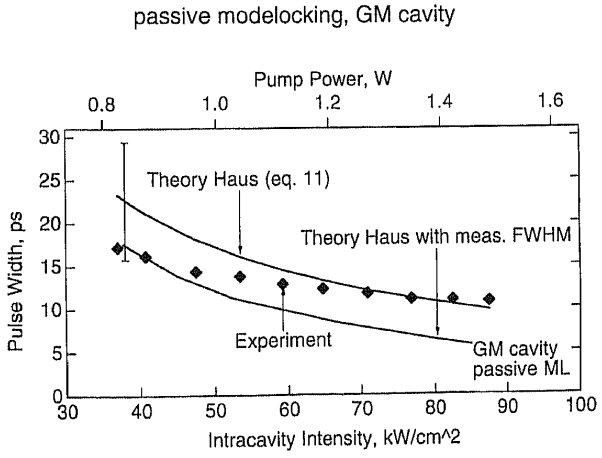

Fig. 10. A-FPSA mode-locked GM Nd:YLF laser ($\lambda = 1047$ nm). Comparison of the measured pulsewidth with the calculated one for the passively mode-locked GM cavity, using Haus' theory for a fast saturable absorber (11). The intracavity intensity I_c is calculated with respect to the mode area in the crystal (i.e., $90 \times 130\ \mu m^2$). The experimental parameters are $\Delta f_g = 360$ GHz [27] (*solid line*) or the measured intensity-dependent lasing gain bandwidth (Fig. 9) (*dashed line*), $\gamma = 2.3 \times 10^{-12}$ cm^2/W and $W = I_c A_{eff,gain}/f_{rep} A_{eff,A-FPSA}$, where $A_{eff,gain} = 3.67 \times 10^{-4}$ cm^2 is the mode area in the laser crystal, $A_{eff,A-FPSA} = 0.28 \times 10^{-4}$ cm^2 the mode area on the saturable absorber, and $f_{rep} = 250$ MHz the pulse repetition rate

5 Actively and passively mode-locked lasers with enhanced SHB

In addition to exhibiting enhanced cw SHB, GE cavities can experience SHB in mode-locked operation, when the pulse overlaps with itself at the end mirror, allowing for SHB within the gain region. Figure 11 shows the measured pulsewidth and bandwidth for all cavities vs the

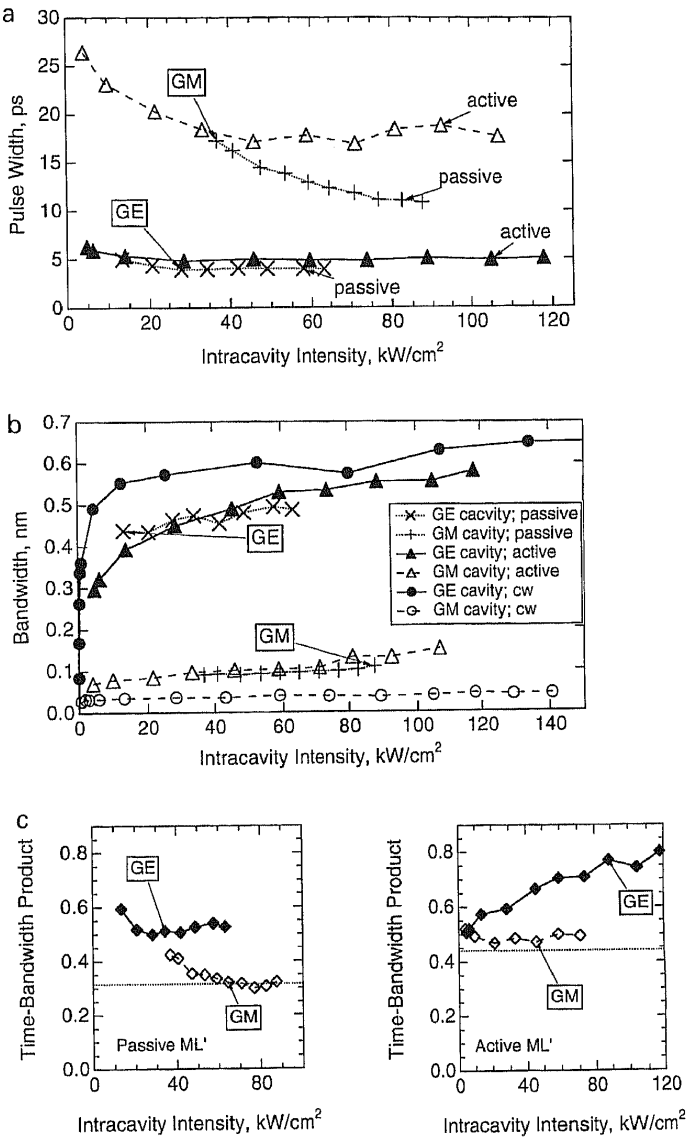

Fig. 11. a Pulse widths of A-FPSA and acousto-optically mode-locked Nd:YLF laser in the GE- and GM-cavity configuration. Pulsewidths about three times shorter are achieved with the GE-cavity configuration due to enhanced SHB. **b** CW, actively and passively mode-locked lasing spectra as function of the intracavity intensity. **c** Time–bandwidth product for the actively (*right*) and passively (*left*) mode-locked Nd:YLF laser in the GE- and GM-cavity configuration. Enhanced SHB results in shorter, but not transform-limited pulses if Gaussian or sech^2 pulses are assumed. The *dashed line* shows the ideal time–bandwidth product assuming a sech^2 pulse form for passive mode locking and Gaussian pulse form for active mode locking. In **a**–**c**, the intracavity intensity is calculated in the laser crystal

average intracavity intensity inside the crystal. Active mode locking in the GE cavity routinely achieves pulses around 5 ps (Fig. 11a), in contrast to the 17 ps pulses for the GM cavity (Fig. 8). Thus, the GE cavity shows significant additional pulse shortening by approximately a factor 3, which cannot be explained by the Kuizenga-Siegman (2) and the Haus theory (6), even including the intensity-dependent gain bandwidth (Figs. 8, 9). In addition, the same basic behavior was observed with a passively mode-locked Nd:YLF laser using an A-FPSA (Fig. 11). In this case, the pulse widths are 11 ps for the GM cavity (Fig. 10) and 4 ps for the GE cavity (Fig. 11a). For the GE cavity, the mode-locked time–bandwidth product is ≈ 1.6–2.2 times above the ideal product for a sech^2 pulse shape, while the GM cavity has nearly ideal time–bandwidth-limited performance (Fig. 11c). The time–bandwidth product for the GE cavity could not be improved by external dispersion compensation.

In addition to shorter pulse widths, we also have measured a substantially shorter mode-locking build-up time for the GE cavity compared to the GM cavity for a given small-signal gain (Fig. 12), for both active and passive mode locking. Additionally, the starting behavior is more stable, i.e., no Q-switching is observed in the case of the GE cavity, whereas the GM cavity typically showed transient Q-switching behavior before steady-state mode locking was reached. The mode-locking build-up time for passive mode locking is ≈ 1 ms, for active mode locking less than 100 μs. The faster mode–locking build-up time in the actively mode–locked laser is due to the much stronger mode–locking driving force during build-up, as discussed before [34]. Because of the higher pulse repetition rate, which decreases the mode-locking driving force, the 1 ms mode locking build-up time is longer than previously published values [35].

The shorter pulse widths and build-up times of GE cavities can also be qualitatively explained as follows. In the traditional picture of mode locking, the mode-locker, be it an active modulator or a passive saturable absorber, effectively reduces the gain at the line center so that the other axial modes can reach threshold. This means that the mode-locker has to "force" energy from the axial modes near the line center into modes farther from the line centre. We have shown schematically in Fig. 2 and theoretically in Part II of this paper ([1], Sect. 3) that enhanced SHB effectively flattens the saturated gain profile due to strong axial mode coupling via the gain grating. In the GE cavity, several widely spaced axial modes are already running in cw lasing (Figs. 5, 11b). The mode-locker forces other axial modes to lase around each of these initial axial modes. The mode-locker only needs to force enough other axial modes to lase until these groups of modes overlap and phase lock together through an effective injection seeding. This requires much less modulation strength than conventional mode locking in a laser with homogeneously broadened gain. A given mode-locker, then, can phase lock a much broader spectrum and generate shorter pulses in the GE cavity compared to a GM cavity. This also explains the experimental observation that the final pulse width does neither depend strongly on the mode-locker or on the saturable absorber modulation depth nor on SPM [1] (Fig. 11a). Furthermore, the GE cavity generates similar pulse durations for both active and passive mode locking.

In Part II of this paper [1], we will show that the larger time–bandwidth product in the GE cavity (Fig. 11c) is mainly due to the flat gain produced by enhanced SHB. This results in a lasing spectrum that is no longer Gaussian or sech^2, and the pulses cannot be easily shortened by external dispersion compensation.

It is also interesting to note that weak SHB in a GM cavity can be responsible for starting difficulties in a KLM laser [36, 37] due to spurious reflections on the gain grating which are caused by the standing-wave pattern. The same effect was observed in a ring laser where both counter propagating waves were present [38]. In our case, however, the mode-locking driving force is significantly stronger than for KLM [33], and SHB strongly reduces the mode-locking build-up time (Fig. 12).

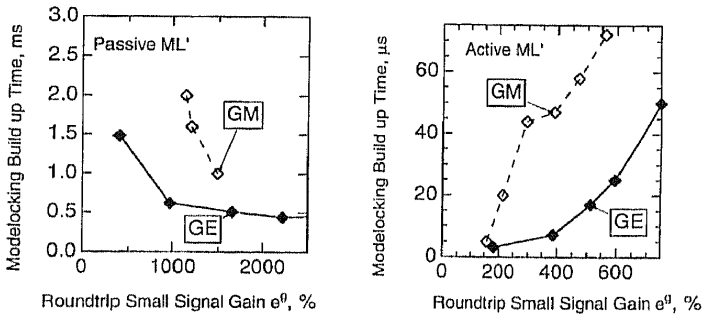

Fig. 12. Mode-locking build-up time for A-FPSA (*left*) and acousto-optic mode-locked (*right*) Nd:YLF laser as function of the small-signal gain. Self-starting is always faster and more stable (no intermediate Q-switching) in the GE-cavity configuration

6 Conclusion

We have investigated the influence of SHB by comparison of a GE with a GM cavity for cw, active and passive mode locking. We found the cw mode spacing between running modes in the GE cavity to be given approximately by the free spectral range of the crystal, as long as the absorption length is not more than an order of magnitude smaller than the crystal length. For both active and passive mode locking, significantly shorter pulse widths (≈ 3 times) are achieved in a GE cavity in comparison to a GM cavity. Additionally, the time–bandwidth product is about twice the ideal product for a sech^2 pulse shape and cannot be improved by intracavity dispersion compensation, because it is primarily due to the flattened gain. We conclude that for the GE cavity, the influence of SHB is the main reason for the observed pulsewidth reduction in diode-pumped and other longitudinally pumped picosecond Nd-doped laser systems. The theory confirming the effects of SHB is given in Part II of this paper [1].

Acknowledgements. We would like to thank G. Huber and J.-P. Meyn for the Nd:LSB crystal, G. Huber for helpful discussions concerning the temperature broadening of the fluorescence bandwidth, T.H. Chiu for growing the A-FPSA and Lightwave Electronics for the acousto-optic mode-locker. This work was supported by the Swiss priority program in Optics under contract number 317.

References

1. F.X. Kärtner, B. Braun, U. Keller: Appl. Phys. B **61** (1995) Part II of this paper (in press)
2. D.J. Kuizenga, A.E. Siegman: IEEE J. QE-**6**, 694 (1970)
3. D.J. Kuizenga, A.E. Siegman: IEEE J. QE-**6**, 709 (1970)
4. U. Keller, K.J. Weingarten, K.D. Li, D.C. Gerstenberger, P.T. Khuri-Yakub, D.M. Bloom: Opt. Lett. **15**, 45 (1990)
5. K.J. Weingarten, D.C. Shannon, R.W. Wallace, U. Keller: Opt. Lett. **15**, 962 (1990)
6. G.T. Maker, A.I. Ferguson: Appl. Phys. Lett. **54**, 403 (1989)
7. A.A. Godil, A.S. Hou, B.A. Auld, D.M. Bloom: Opt. Lett. **16**, 1765 (1991)
8. H.A. Haus, Y. Silberberg: IEEE J. QE-**22**, 325 (1986)
9. M. Sargent: Appl. Phys. **9**, 127 (1976)
10. C.L. Tang, H. Statz, G. DeMars: J. Appl. Phys. **34**, 2289 (1963)
11. C.S. Adams, G.T. Maker, A.I. Ferguson: Opt. Commun. **76**, 127 (1990)
12. P.A. Schulz, S.R. Henion: Opt. Lett. **16**, 1502 (1991)
13. U. Keller, T.H. Chiu, J.F. Ferguson: CLEO (1993), paper JWA4
14. B. Braun, K.J. Weingarten, U. Keller: CLEO (1994), paper CTHI1
15. C.J. Flood, D.R. Walker, H.M.v. Driel: Opt. Lett. **20**, 58 (1995)
16. A.E. Siegman: *Lasers* (Univ. Science Books, Mill Valley, CA 1986)
17. V.R. Mironenko: Sov. J. Quantum Electron. **10**, 1203 (1980)
18. G.J. Kintz, T. Baer: IEEE J. QE-**26**, 1457 (1990)
19. J.J. Zayhowski: Opt. Lett. **15**, 431 (1990)
20. U. Keller, D.A.B. Miller, G.D. Boyd, T.H. Chiu, J.F. Ferguson, M.T. Asom: Opt. Lett. **17**, 505 (1992)
21. U. Keller: Appl. Phys. B **58**, 347 (1994)
22. K.J. Weingarten, B. Braun, U. Keller: Opt. Lett. **19**, 1140 (1994)
23. B. Beier, J.-P. Meyn, R. Knappe, K.-J. Boller, G. Huber, R. Wallenstein: Appl. Phys. B **58**, 381 (1994)
24. J.-P. Meyn, T. Jensen, G. Huber: IEEE J. QE-**30**, 913 (1994)
25. A.E. Siegman, D.J. Kuizenga: Optoelectron **6**, 43 (1974)
26. H.A. Haus: J. Appl. Phys. **46**, 3049 (1975)
27. A.A. Kaminskii: *Laser Crystals: Their Physics and Properties*, 2nd edn. Springer Ser. Opt. Sci., Vol 14 (Springer, Berlin, Heidelberg 1981)
28. H.A. Haus: IEEE J. QE-**11**, 323 (1975)
29. F.X. Kärtner, D. Kopf, U. Keller: J. Opt. Soc. Am. B **12**, 486 (1995)
30. W. Koechner: *Solid-State Laser Engineering*, 4th edn. Springer Ser. Opt. Sci., Vol 1 (Springer, Berlin, Heidelberg 1996)
31. F. Salin, J. Squier, M. Piché: Opt. Lett. **16**, 1674 (1991)
32. D. Kopf, K.J. Weingarten, L. Brovelli, M. Kamp, U. Keller: Opt. Lett. **19**, 2143 (1994)
33. L.R. Brovelli, U. Keller, T.H. Chiu: J. Opt. Soc. Am. B **12**, 311 (1995)
34. E.P. Ippen: Appl. Phys. B **58**, 159 (1994)
35. U. Keller, T.H. Chiu, J.F. Ferguson: Opt. Lett. **18**, 217 (1993)
36. K. Tamura, J. Jacobson, E.P. Ippen, H.A. Haus, J.G. Fujimoto: Opt. Lett. **18**, 220 (1993)
37. F. Krausz, T. Brabec: Opt. Lett. **18**, 888 (1993)
38. C.J. Flood, G. Giuliani, H.M.v. Driel: Opt. Lett. **15**, 218 (1990)
39. W. Koechner: *Solid-State Laser Engineering*, 4th edn. Springer Ser. Opt. Sci., Vol 1 (Springer, Berlin, Heidelberg 1996) p. 171
40. G. Quarles: *Lightning Optical*, private communication (1994)